

State and dynamical parameter estimation for open quantum systems

Jay Gambetta and H. M. Wiseman*

School of Science, Griffith University, Brisbane 4111, Australia

Following the evolution of an open quantum system requires full knowledge of its dynamics. In this paper we consider open quantum systems for which the Hamiltonian is “uncertain”. In particular, we treat in detail a simple system similar to that considered by Mabuchi [Quant. Semiclass. Opt. **8**, 1103 (1996)]: a radiatively damped atom driven by an unknown Rabi frequency Ω (as would occur for an atom at an unknown point in a standing light wave). By measuring the environment of the system, knowledge about the system state, and about the uncertain dynamical parameter, can be acquired. We find that these two sorts of knowledge acquisition (quantified by the posterior distribution for Ω , and the conditional purity of the system, respectively) are quite distinct processes, which are not strongly correlated. Also, the quality and quantity of knowledge gain depend strongly on the type of monitoring scheme. We compare five different detection schemes (direct, adaptive, homodyne of the x quadrature, homodyne of the y quadrature, and heterodyne) using four different measures of the knowledge gain (Shannon information about Ω , variance in Ω , long-time system purity, and short-time system purity).

PACS numbers: 03.65.Yz, 42.50.Lc, 03.65.Wj

I. INTRODUCTION

Quantum parameter estimation is a well-established area [1, 2], which is usually formulated as follows. A known quantum state enters an apparatus that performs an operation on the state. The operation, which is usually unitary but need not be [3, 4], is parameterized by one or more unknown parameters. The goal is to estimate these parameters by making a measurement on the (unknown) output state. Except in special cases, it is not possible precisely to find out the unknown parameters from a measurement on a single system. Rather, the operation and measurement must be performed repeatedly, on a sequence of identically prepared quantum systems.

There is a trivial sense in which it is possible to obtain complete information about the unknown parameters from a single system. That is by taking the output state after the measurement, and using it as the next input state, having perhaps transformed it first. If the transformation required is as difficult as preparing a new system from scratch, then there is nothing to be gained by reusing the same system. However, this scenario of repeated measurements on a single system is useful pedagogically to make the transition to continuously monitored systems with unknown dynamical parameters. This transition is made by considering the limit where the unknown transformation is infinitesimally different from the identity, and the repeat time is infinitesimal.

To the best of our knowledge, a theoretical treatment of estimating an unknown dynamical parameter by continuous observation of a system was first done by Mabuchi [5]. His system was a two-level atom coupled to a classically driven electromagnetic field mode in a cavity.

The unknown parameter was the position of the atom. This is a dynamical parameter because it determines the strength of the coupling between the atom and field (the Rabi frequency). The continuous monitoring considered was counting the photons that escape through one of the cavity mirrors. Mabuchi used Bayesian statistics to determine the posterior probability distribution for the Rabi frequency. This represents the knowledge the experimenter would have about the Rabi frequency given a particular (typical) measurement record. The measurement is continuous in time (monitoring) because in any instant of time a photon may or may not be detected.

In this paper we are concerned with the same question, namely how would an experimenter gain knowledge of an unknown dynamical parameter from the measurement record resulting from monitoring the system. We even choose a similar (but even simpler) quantum system to that of Ref. [5], namely an atom driven by a classical field of unknown Rabi frequency. However, our analysis goes beyond, and has additional aims to, that of Ref. [5] (although we should note that extensions similar to the first three outlined below were suggested in a footnote of that work.)

First, we consider the entire ensemble of possible measurement records and parameter values, rather than just one (typical) measurement record from one parameter value.

Second, we quantitatively characterize this ensemble by calculating the average information gained (in bits) by the measurement, as a function of time.

Third, we consider different ensembles resulting from different measurement schemes on the system. We emphasize that the choice of measurement scheme does not affect the evolution of the system on average. That is, for all measurement schemes, averaging over the possible results and the possible values of the Rabi frequency yields the same equation of motion for the system state. Physically, this is because the average behaviour of the system

*Electronic address: h.wiseman@gu.edu.au

is determined by its immediate environment, whereas the different measurement schemes are effected by detecting the light emitted by the system in different ways. However, the different measurement schemes give very different typical posterior distributions, and very different rates of information gain.

Fourth, and perhaps most distinctively, we consider not just the estimation of the unknown parameter, but also the estimation of the state of the system conditioned on the measurement results [6]. We do this using the same Bayesian method as for the parameter estimation. In this respect, our work could be seen as an extension of quantum trajectory theory [7] to systems with unknown dynamical parameters. Quantum trajectory theory is simply the application of quantum measurement theory to continuous monitoring of open quantum systems, most usually optical systems subject to photodetection [8].

If the dynamical parameters for an open quantum system are known then conditioning the system on efficient detection of its emissions is guaranteed to monotonically increase its average purity in time, as information is gained about the system. But if dynamical parameters are not known then the average purity may decrease, as the different possible evolutions are summed incoherently. On the other hand, the measurement record also contains information about these parameters, so that these parameters become better defined over time. Hence one might expect that the system will eventually become pure anyway.

It is one of the main results of this paper that this expectation is not met. For our system there are some monitoring schemes for which the parameter never becomes sufficiently well known for the system state to become pure. However, there is no simple correlation between the information gained about the parameter (the Rabi frequency) and the final purity of the system (the atom). One monitoring scheme yields almost no parameter information, yet produces, on average, a much purer final system state than do other schemes that yield large amounts of parameter information. Moreover, the rates at which the system state purifies is, for some monitoring schemes, tied to the rate of parameter information gain, while for other monitoring schemes it is much faster than that. These results can be understood only from an appreciation of the conditional dynamics induced by the different detection schemes.

The remainder of this paper is organized as follows. In Sec. II we present the general formalism for state and dynamical parameter estimation by monitoring a single system. We also explain how the parameter information gained is quantified. In Sec. III we introduce the system to which we apply our formalism, a two-level atom, driven by an unknown Rabi frequency, and monitored by having its fluorescence detected. Sec. IV contains the results of our numerical simulations of the relevant ensemble averages for five different detection schemes: direct, the adaptive scheme of Wiseman and Toombes [9], homodyne of the x quadrature, homodyne of the y quadrature,

and heterodyne. Sec. V concludes.

II. GENERAL FORMALISM

A. Quantum trajectories

It is well known that quantum trajectories can be used to describe the evolution of a continuously monitored open system [8]. Since here we are continuously monitoring an open system with an unknown dynamical parameter, we begin by giving a brief outline of the standard quantum trajectory theory.

A good place to start is with the measurement formalism for open systems [10, 11]. An open system is simply a quantum system that interacts with its environment (usually called a bath). This interaction, like all quantum interactions, generally entangles the system and the bath. If we initially have states $|\psi(t_0)\rangle$ and $|m(t_0)\rangle$ for the system and bath respectively, and let these states entangle by $U(t_0 + T)$, a unitary operator which includes both the bath-system coupling and the system dynamics. An instantaneous rank-one projective measurement on the bath will result in the state after the measurement being

$$|r\rangle |\psi_r(t_0 + T)\rangle = \frac{|r\rangle \langle r| U(t_0 + T) |m(t_0)\rangle |\psi(t_0)\rangle}{\sqrt{P(r)}}, \quad (2.1)$$

where $P(r)$ is the probability of getting the result r . Eq. (2.1) shows that after the measurement the system and the bath are disentangled, so it is not necessary to continue to describe the bath in our treatment of the measurement. This allows Eq. (2.1) to be reduced to

$$|\psi_r(t_0 + T)\rangle = \frac{M_r(T) |\psi(t)\rangle}{\sqrt{P(r)}}, \quad (2.2)$$

where $M_r(T) = \langle r| U(t_0 + T) |m(t_0)\rangle$ is called the measurement operator and has the feature of collapsing the observer's knowledge of the system into a state that is consistent with the result r . $M_r(T)$ is still an operator for the system as $U(t_0 + T)$ is an operator on the tensor product Hilbert space for system and the bath. It is important to note that this measurement operator is not necessarily a projector in the system Hilbert space.

The probability $P(r)$ is given by

$$P(r) = \text{Tr}[F_r(T) |\psi(t_0)\rangle \langle \psi(t_0)|], \quad (2.3)$$

where F_r is called the effect and is defined as

$$F_r(T) = M_r^\dagger(T) M_r(T). \quad (2.4)$$

The complete set of effects must sum to one:

$$\sum_r F_r(t) = 1. \quad (2.5)$$

The above formalism for measurement only considers pure states, but to take into account initially mixed states Eq. (2.2) can be rewritten in terms of the state matrix. The state after the measurement is then

$$\rho_r(t_0 + T) = M_r(T)\rho(t_0)M_r^\dagger(T)/P(r). \quad (2.6)$$

Here Eq. (2.6) describes the state conditioned on the result r and is referred to as an *unraveling* of the average post-measurement state $\rho(t_0 + T)$. That is, the weighted mean of all the possible conditioned states for one unraveling is equal to the average state:

$$\rho(t_0 + T) = \mathbb{E}[\rho_r(t_0 + T)] = \sum_r P(r)\rho_r(t_0 + T). \quad (2.7)$$

It should be noted that an average state has more than one unraveling. The different unravelings correspond to different sets of measurement operators, arising from different sets of environment projectors $|r\rangle\langle r|$ in Eq. (2.1).

As mentioned earlier, quantum trajectories arises when this measurement formalism is applied to a continuously monitored open system [8]. In continuous monitoring, repeated measurements of duration δt are performed on the state. This results in the state being conditioned on a record $\mathbf{I}_{[0,t]}$, which is a string containing the results r_k of each measurement. Here the subscript k refers to a measurement at time $t_k = k\delta t$, with $t_0 = 0$. Using this $\mathbf{I}_{[0,t]}$, the conditioned state at time t can be written as

$$\rho_{\mathbf{I}}(t) = \tilde{\rho}_{\mathbf{I}}(t)/P(\mathbf{I}_{[0,t]}), \quad (2.8)$$

where $\tilde{\rho}_{\mathbf{I}}(t)$ is an unnormalized state conditioned on $\mathbf{I}_{[0,t]}$ and is equal to

$$\begin{aligned} \tilde{\rho}_{\mathbf{I}}(t) \\ = M_{r_k}M_{r_{k-1}}\dots M_{r_1}\rho(0)M_{r_1}^\dagger\dots M_{r_{k-1}}^\dagger M_{r_k}^\dagger. \end{aligned} \quad (2.9)$$

The probability of obtaining this record is

$$P(\mathbf{I}_{[0,t]}) = P(r_k)P(r_{k-1})\dots P(r_1) = \text{Tr}[\tilde{\rho}_{\mathbf{I}}(t)]. \quad (2.10)$$

To completely achieve continuous monitoring we let the time step between measurements, δt , tend towards the infinitesimal interval dt . In doing this, Eq. (2.8) defines a stochastic master equation (SME), with its ensemble average reproducing the usual deterministic master equation. That is,

$$\begin{aligned} \rho(t) &= \sum_{\mathbf{I}_{[0,t]}} P(\mathbf{I}_{[0,t]})\rho_{\mathbf{I}}(t) = \sum_{\mathbf{I}_{[0,t]}} \tilde{\rho}_{\mathbf{I}}(t) \\ &= \lim_{\delta t \rightarrow 0} \sum_{r_t/\delta t \dots r_1} M_{r_t/\delta t} \dots M_{r_1}\rho(0)M_{r_1}^\dagger \dots M_{r_t/\delta t}^\dagger \\ &= \lim_{\delta t \rightarrow 0} (1 + \mathcal{L}\delta t)^{t/\delta t} \rho(0) = \exp(\mathcal{L}t)\rho(0), \end{aligned} \quad (2.11)$$

where for arbitrary ρ , \mathcal{L} is the Liouvillian superoperator defined as $\mathcal{L}\rho = \lim_{\delta t \rightarrow 0} (\sum_r M_r \rho M_r^\dagger - \rho)/\delta t$.

B. Quantum trajectories with an unknown parameter

We now consider the situation where there is an unknown dynamical parameter λ in \mathcal{L} , and hence in the measurement operators M_r . This is done by simply noting that for each λ there will be a conditioned state. This gives a doubly conditioned state of the form

$$\rho_{\mathbf{I},\lambda}(t) = \tilde{\rho}_{\mathbf{I},\lambda}(t)/P(\mathbf{I}_{[0,t]}|\lambda), \quad (2.12)$$

where $P(\mathbf{I}_{[0,t]}|\lambda)$ is the probability of getting $\mathbf{I}_{[0,t]}$ given λ . It is obtained by

$$P(\mathbf{I}_{[0,t]}|\lambda) = \text{Tr}[\tilde{\rho}_{\mathbf{I},\lambda}(t)]. \quad (2.13)$$

We wish to determine the posterior probability distribution $P(\lambda|\mathbf{I}_{[0,t]})$ of λ , given $\mathbf{I}_{[0,t]}$. This can be achieved using a Bayesian inference formula [12].

$$P(\lambda|\mathbf{I}_{[0,t]}) = \frac{P(\mathbf{I}_{[0,t]}|\lambda)P_0(\lambda)}{\int P(\mathbf{I}_{[0,t]}|\lambda)P_0(\lambda)d\lambda}, \quad (2.14)$$

where $P_0(\lambda)$ is the prior distribution for λ . For a ‘‘good measurement’’ of λ , as time increases, we would expect this prior distribution to converge to a δ -distribution.

Theoretically, Eq. (2.14) is complete for determining $P(\lambda|\mathbf{I}_{[0,t]})$. However, in general $P(\mathbf{I}_{[0,t]}|\lambda)$ is very small and in numerical simulations it will incur large computer roundoff errors. The small magnitude of $P(\mathbf{I}_{[0,t]}|\lambda)$ is due to the many possible trajectories the system could follow.

To overcome this problem, linear quantum trajectories [13] were used. Linear quantum trajectories arise if we assume an ostensible distribution for the result r , $\Lambda(r)$ [8]. These $\Lambda(r)$ are independent of λ and the only condition they must satisfy is that they add to one. With these ostensible probabilities, the linear stochastic master equation (LSME) is derived from [8]

$$\bar{\rho}_{\mathbf{I},\lambda}(t) = \tilde{\rho}_{\mathbf{I},\lambda}(t)/\Lambda(\mathbf{I}_{[0,t]}), \quad (2.15)$$

where the ostensible probability for getting $\mathbf{I}_{[0,t]}$ is

$$\Lambda(\mathbf{I}_{[0,t]}) = \Lambda(r_k)\Lambda(r_{k-1})\dots\Lambda(r_1). \quad (2.16)$$

The actual probability of getting $\mathbf{I}_{[0,t]}$ is [8]

$$P(\mathbf{I}_{[0,t]}|\lambda) = \Lambda(\mathbf{I}_{[0,t]})\text{Tr}[\bar{\rho}_{\mathbf{I},\lambda}(t)]. \quad (2.17)$$

Substituting $P(\mathbf{I}_{[0,t]}|\lambda)$ into Eq. (2.14) we obtain

$$P(\lambda|\mathbf{I}_{[0,t]}) = \frac{\text{Tr}[\bar{\rho}_{\mathbf{I},\lambda}(t)]P_0(\lambda)}{\int \text{Tr}[\bar{\rho}_{\mathbf{I},\lambda}(t)]P_0(\lambda)d\lambda}. \quad (2.18)$$

From Eq. (2.18) we see that to calculate $P(\mathbf{I}_{[0,t]}|\lambda)$, the norm of the linear conditioned state [Eq. (2.15)] is needed. The order of magnitude of this norm is dependent on the ostensible probability we chose. By Eq. (2.17), if $\Lambda(\mathbf{I}_{[0,t]})$ is chosen to be of the same order as the true probability, this norm will be of order unity. This avoids the problem of large computer roundoff error.

C. Quantifying the information gained

One of the main aims of this paper is to classify the information gained about the unknown parameter. The posterior probability calculated by Eq. (2.18) contains all the information about λ for a particular record. However the question remains, how can this information be quantified? Two measures were investigated. The first is the variance:

$$V_{\mathbf{I}} = \int P(\lambda|\mathbf{I}_{[0,t]})\lambda^2 d\lambda - \left(\int P(\lambda|\mathbf{I}_{[0,t]})\lambda d\lambda \right)^2. \quad (2.19)$$

The second is the information gain, $\Delta I_{\mathbf{I}}$ defined as [14]

$$\begin{aligned} \Delta I_{\mathbf{I}} &= \int P(\lambda|\mathbf{I}_{[0,t]}) \log_2 P(\lambda|\mathbf{I}_{[0,t]}) d\lambda \\ &\quad - \int P_0(\lambda) \log_2 P_0(\lambda) d\lambda. \end{aligned} \quad (2.20)$$

This measures the number of bits of information gained by the observer about the parameter λ . It can be thought of as the negative change in entropy of λ . The greatest information gain corresponds to the transition from a flat (most disordered) distribution to a peaked (most ordered) distribution.

These parameters give an indication of the quality of knowledge gained by an observer, for a particular run of the experiment. To characterize a particular measurement scheme, it is necessary to calculate the ensemble averages of $V_{\mathbf{I}}$ and $\Delta I_{\mathbf{I}}$, which we denote as V and ΔI . The ensemble average of a parameter $A_{\mathbf{I}}$ is defined as

$$\begin{aligned} A &= E[A_{\mathbf{I}}] = \sum_{\mathbf{I}_{[0,t]}} A_{\mathbf{I}} P(\mathbf{I}_{[0,t]}) \\ &= \sum_{\mathbf{I}_{[0,t]}} \int A_{\mathbf{I}} P(\mathbf{I}_{[0,t]}|\lambda) P_0(\lambda) d\lambda. \end{aligned} \quad (2.21)$$

Numerically, this is done by picking a true λ , λ_{true} , randomly from $P_0(\lambda)$, and then simulating a quantum trajectory for this λ_{true} , yielding $\mathbf{I}_{[0,t]}$. This gives a typical record as would be obtained experimentally. This $\mathbf{I}_{[0,t]}$ is then used to calculate $\text{Tr}[\bar{\rho}_{\mathbf{I},\lambda}(t)]$ for all λ 's in the range of P_0 . This allows the calculation of $P(\lambda|\mathbf{I}_{[0,t]})$, with this probability the parameter of interest $A_{\mathbf{I}}$ can be calculated. By storing this value and repeating the above procedure $n \gg 1$ times, the ensemble average A of $A_{\mathbf{I}}$ is obtained.

D. Best estimate of conditioned state

Another aim of this paper was to determine the best estimate of the state given the knowledge we have obtained from a measurement. In Eq. (2.12) we defined the doubly conditioned state that arose when the state was conditioned on both $\mathbf{I}_{[0,t]}$ and λ . From Eq. (2.12) there are two best estimate states that can be calculated. They

are ρ_{λ} and $\rho_{\mathbf{I}}$ and can be interpreted as the best estimate state, when λ or $\mathbf{I}_{[0,t]}$ is known respectively. They are defined as follows

$$\rho_{\lambda}(t) = \sum_{\mathbf{I}_{[0,t]}} \tilde{\rho}_{\mathbf{I},\lambda}(t), \quad (2.22)$$

$$\rho_{\mathbf{I}}(t) = \frac{\int \tilde{\rho}_{\mathbf{I},\lambda}(t) P_0(\lambda) d\lambda}{\int P(\mathbf{I}_{[0,t]}|\lambda) P_0(\lambda) d\lambda}. \quad (2.23)$$

It should be noted that the average of each of these states will give the same average state $\rho(t)$.

Equation (2.22) describes the best estimate state that arises when the dynamical parameter is known and the record is not (i.e. a non-monitored system). This obeys master equation $\dot{\rho}_{\lambda} = \mathcal{L}_{\lambda}\rho_{\lambda}$. Of more interest to us is the best estimate state described by Eq. (2.23), which is the state conditioned on some observed record $\mathbf{I}_{[0,t]}$, when the true value of λ is unknown.

In calculating $\rho_{\mathbf{I}}$, if we use Eq. (2.23), we again run into the problem that the magnitude of $\tilde{\rho}_{\mathbf{I},\lambda}(t + dt)$ will typically be very small. Again this is overcome by using linear quantum trajectories, replacing Eq. (2.23) by

$$\rho_{\mathbf{I}}(t) = \frac{\int \tilde{\rho}_{\mathbf{I},\lambda}(t) P_0(\lambda) d\lambda}{\int \text{Tr}[\bar{\rho}_{\mathbf{I},\lambda}(t)] P_0(\lambda) d\lambda}. \quad (2.24)$$

To quantify the information gained about the state, the purity ($p_{\mathbf{I}}$) can be determined,

$$p_{\mathbf{I}} = \text{Tr}[\rho_{\mathbf{I}}(t)^2]. \quad (2.25)$$

The ensemble average purity ($p = E[p_{\mathbf{I}}]$) will give us an indication of how well the measurement scheme is at producing pure states. One might expect that a high p would correspond to a high ΔI . However it will be seen that this is not true.

III. THE SYSTEM

The system we are considering is a classically driven two level atom, immersed in the vacuum. With no monitoring of the vacuum field, the average state evolution when all the dynamical parameters are known is given by the master equation. The Lindblad form [15] of the master equation for the TLA, in the interaction picture (with respect to the free evolution of the atom) is [16]

$$\dot{\rho}(t) = -\frac{i\Omega}{2}[\sigma_x, \rho(t)] + \gamma\mathcal{D}[\sigma]\rho(t) = \mathcal{L}_{\Omega}\rho(t). \quad (3.1)$$

Here Ω is the Rabi frequency, γ is the spontaneous emission rate, σ is the lowering operator, σ_x is the usual Pauli matrix and \mathcal{D} is the superoperator that represents damping of the system into the environment. It is defined as [17]

$$\mathcal{D}[a]\rho = a\rho a^\dagger - \frac{1}{2}\{a^\dagger a\rho + \rho a^\dagger a\}. \quad (3.2)$$

The solution of this equation can be described by the Bloch vectors (x, y, z) , with ρ written as

$$\rho = \frac{1}{2}(1 + x\sigma_x + y\sigma_y + z\sigma_z). \quad (3.3)$$

The purity p is equal to

$$p = \frac{1}{2}(1 + x^2 + y^2 + z^2), \quad (3.4)$$

Using this Bloch representation the solution of Eq. (3.1) is a state that rotates about the x -axis at frequency Ω , with damping in all variables towards the steady state value of

$$x_{ss} = 0, \quad y_{ss} = \frac{2\Omega\gamma}{2\Omega^2 + \gamma^2}, \quad z_{ss} = \frac{-\gamma^2}{2\Omega^2 + \gamma^2}. \quad (3.5)$$

The most obvious choice for the unknown dynamical parameter is Ω , as indicated by the subscript in \mathcal{L}_Ω in Eq. (3.1). This can be physically motivated as follows: if we placed a laser-cooled atom (with no center-of-mass motion) in a classical standing field, then the Ω it would experience is

$$\Omega = \Omega_{\max} \sin(kx), \quad (3.6)$$

where k is the wavevector for the classical field and x is the position of center of mass of the atom. We assume that the placement of the atom in the field is not biased in any way. That is, in one wavelength (λ) of the field the atom position distribution is given by $P_0(x) = 1/\lambda$. Using Eq. (3.6), $P_0(x)$ can be transformed into a probability distribution in Ω space,

$$P_0(\Omega) = \frac{1}{\pi\sqrt{\Omega_{\max}^2 - \Omega^2}}. \quad (3.7)$$

This is the prior distribution for Ω , that will be used in the rest of this paper, with $\Omega_{\max} = 10\gamma$. Along with this prior distribution the initial condition that we will use for our simulations, unless otherwise stated, is $\rho_{\mathbf{I},\Omega}(0)$ satisfying

$$\mathcal{L}_\Omega \rho_{\mathbf{I},\Omega}(0) = 0. \quad (3.8)$$

That is, we will assume the initial state is the steady state of the general master equation Eq. (3.1).

IV. RESULTS

The results of this paper are broken down into five subsections, each corresponding to one of the five measurement schemes investigated.

A. Direct Detection

The first measurement scheme investigated was direct detection. This involves the detection of all the fluorescence emitted by the atom as shown in Fig. 1. Continuous monitoring with this detection scheme will yield

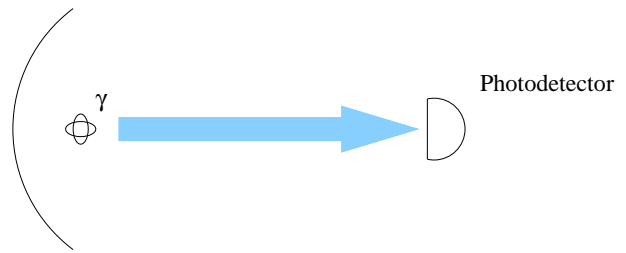


FIG. 1: A schematic for direct detection. The atom is placed at the focus of a parabolic mirror so that all the fluorescence emitted by the atom is detected by the photodetector.

either one of two results for each interval dt , a detection (labelled by a 1) or no detection (labelled by a 0). Thus $\mathbf{I}_{[0,t]}$ will be a string of 0's and 1's. The measurement operators for each of these results are [8]

$$M_1(dt) = \sqrt{dt\gamma} \sigma, \quad (4.1)$$

$$M_0(dt) = 1 - \left(i\frac{\Omega}{2}\sigma_x + \frac{\gamma}{2}\sigma^\dagger\sigma \right) dt. \quad (4.2)$$

It can be shown that these measurement operators satisfy the completeness condition, Eq. (2.5). Using these measurement operators and Eq. (2.8), a SME for direct detection can be written as

$$d\rho_{\mathbf{I},\Omega} = dN(t)\mathcal{G}[\sqrt{dt\gamma}\sigma]\rho_{\mathbf{I},\Omega} - dt\mathcal{H}\left[i\frac{\Omega}{2}\sigma_x + \frac{\gamma}{2}\sigma^\dagger\sigma\right]\rho_{\mathbf{I},\Omega}, \quad (4.3)$$

where \mathcal{G} and \mathcal{H} are the nonlinear superoperators defined for arbitrary a and ρ by

$$\mathcal{G}[a]\rho = \frac{a\rho a^\dagger}{\text{Tr}[a\rho a^\dagger]} - \rho, \quad (4.4)$$

$$\mathcal{H}[a]\rho = a\rho + \rho a^\dagger - \text{Tr}[a\rho + \rho a^\dagger]\rho. \quad (4.5)$$

In Eq. (4.3), the variable dN is a stochastic increment that equals one if there is a detection in the interval dt and equals 0 otherwise. Formally, dN is defined by

$$dN(t)^2 = dN(t), \quad (4.6)$$

$$E[dN(t)] = P(1) = dt\gamma \langle \sigma^\dagger\sigma \rangle. \quad (4.7)$$

By averaging Eq. (4.3) and using Eq. (4.7), it is easily seen that the SME is an unraveling of the general master equation, Eq. (3.1). A typical trajectory of this SME is shown in Fig. 2 (solid line), for $\Omega = 5\gamma$. It is observed that the x component is zero, and the y and z oscillate in quadrature. This can be understood physically as the state is dominated by the $\Omega\sigma_x/2$ Hamiltonian, with detections occurring stochastically according to Eq. (4.7). After each detection the state collapses to the ground state ($x = 0$, $y = 0$, and $z = -1$).

To consider the case when Ω is unknown, a LSME had to be developed. Using the direct detection measurement operators and Eq. (2.15), with $\Lambda(r)$ defined as

$$\Lambda(1) = \epsilon dt = 1 - \Lambda(0), \quad (4.8)$$

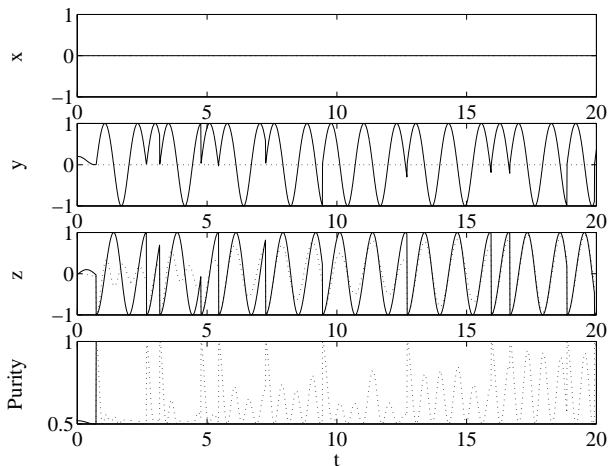


FIG. 2: The best estimate states when Ω is known (Solid line) and unknown (dotted line) for $\Omega_{\text{true}} = 5\gamma$ when direct detection is used. Time is measured in units of γ^{-1} , x , y , and z are the Bloch vector components and the purity $p = \frac{1}{2}(1 + x^2 + y^2 + z^2)$. The initial states are the steady state for the known case and the average steady state for the unknown case.

where ϵ is an arbitrary parameter, the LSME is

$$d\bar{\rho}_{\mathbf{I},\Omega} = dN(t)\bar{\mathcal{G}}[\sqrt{dt}\gamma\sigma]\bar{\rho}_{\mathbf{I},\Omega} - dt\bar{\mathcal{H}}[i\frac{\Omega}{2}\sigma_x + \frac{\gamma}{2}\sigma^\dagger\sigma - \frac{\epsilon}{2}]\bar{\rho}_{\mathbf{I},\Omega}. \quad (4.9)$$

The $\bar{\mathcal{G}}$ and $\bar{\mathcal{H}}$ linear superoperators are defined as

$$\bar{\mathcal{G}}[a]\bar{\rho} = \frac{a\bar{\rho}a^\dagger}{\epsilon dt} - \bar{\rho}, \quad (4.10)$$

$$\bar{\mathcal{H}}[a]\bar{\rho} = a\bar{\rho} + \bar{\rho}a^\dagger. \quad (4.11)$$

To obtain the general master equation from Eq. (4.9), $E[dN] = \Lambda(1)$ has to be used. However, to determine the parameters of interest to us, namely $\rho_{\mathbf{I}}(t)$ and $P(\Omega|\mathbf{I}_{[0,t]})$, Eq. (4.9) is numerically simulated for all possible Ω in $P_0(\Omega)$ with dN specified by $\mathbf{I}_{[0,t]}$. This record would ideally be obtained experimentally but for the purpose of this paper it is calculated by numerically evaluating Eq. (4.3) for a known Ω , which we will refer to as Ω_{true} . This $\mathbf{I}_{[0,t]}$ is then used in Eq. (4.9) to generate $\text{Tr}[\bar{\rho}_{\mathbf{I},\Omega}]$ for all the Ω 's between $-\Omega_{\text{max}}$ and Ω_{max} . Then with Eq. (2.24) and Eq. (2.18) one can obtain both $\rho_{\mathbf{I}}(t)$ and $P(\Omega|\mathbf{I}_{[0,t]})$.

For a $\mathbf{I}_{[0,t]}$ based on $\Omega_{\text{true}} = 5\gamma$ the best estimate state and the posterior distribution were calculated and are shown in Fig. 2 and 3 respectively. It is observed that, in contrast to the known Ω case, the best estimate of y is identically zero. This is because positive and negative Ω are initially equally likely, so that y_{ss} in Eq. (3.5) averages to zero. Moreover, the sign of Ω is not determinable by this measurement scheme, because the rate of detections depends only on z , which is independent of the sign of Ω .

Another difference apparent with the unknown Ω case is that z oscillates with a different frequency to the known

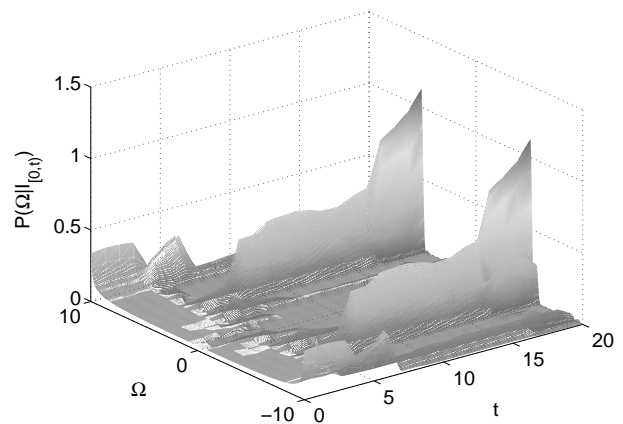


FIG. 3: A plot of a typical $P(\Omega|\mathbf{I}_{[0,t]})$ when $\Omega_{\text{true}} = 5$ for the direct detection scheme. Ω is measured in units of γ and time is measured in units of γ^{-1} .

Ω case, in this case a faster frequency [since $P_0(\Omega)$ is peaked at the end points $|\Omega| = \Omega_{\text{max}} = 10\gamma$]. However as time increases its frequency tends to that of the known case. This is due to the fact that for direct detection the rate of detections is dependent on the magnitude of Ω , so as time goes on one would expect to gain more information about the magnitude of Ω .

These interpretations of the conditioned dynamics are confirmed in Fig. 3. With increasing time, the posterior distribution localizes at $\pm\Omega_{\text{true}}$. The mean is always zero and thus is not an unbiased estimator of Ω . The reason that the magnitude is determinable and the sign is not, can be formulated as follows. In the Bloch representation of Eq. (4.9), with the transformation $y \rightarrow -y$, $\Omega \rightarrow -\Omega$ the equations stay invariant. Since this transformation changes the direction of rotation around the x -axis, we will call it the rotation transformation.

With an indeterminable direction of rotation and this measurement scheme, it can be seen that the best estimate state will never become more pure than a state that is a mixture of two states that rotate in opposite directions around the $x = 0$ great circle of the Bloch sphere. Thus the best estimate state oscillates up and down the z -axis of the Bloch sphere.

We turn now to quantifying the measurement scheme's ability to gain knowledge, by numerically determining the ensemble average purity, V and ΔI . These ensemble averages were calculated for Ω_{true} 's weighted on the prior distribution, Eq. (3.7). These numerical simulations are depicted in Fig. 4 for two initial states; one is the steady state (solid line) and the other is the ground state (dotted line). It is observed that in both cases the average purity of the state never attains one, with the purity in the second case initially decreasing from one. The long time purity ($\simeq 0.75$) is due to the best estimate being a mixture of two states as explained above. This figure can be obtained analytically, if we make the following two assumptions. The first is that $\Omega_{\text{true}} \gg \gamma$. This is valid as $P_0(\Omega)$

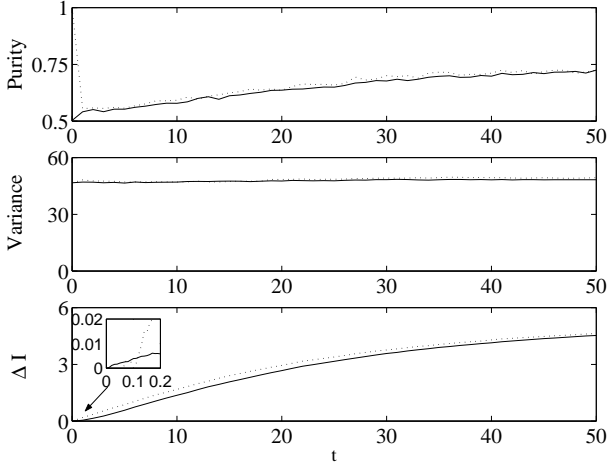


FIG. 4: The ensemble average ($n = 1000$) of the purity, variance and ΔI when direct detection is used, for two initial states, the steady state (solid) and ground state (dotted). Time is measured in units of γ^{-1} .

from which Ω_{true} is drawn is peaked at $\pm\Omega_{\text{max}}$, and in our calculations $\Omega_{\text{max}} \gg \gamma$. The second assumption is that in the long time limit the posterior distribution localizes on $\pm\Omega_{\text{true}}$, which is what is seen in Fig. 3. With these two assumption the long-time best estimate state in Bloch representation will be

$$x = 0, \quad y = 0, \quad z \simeq -\cos \Omega_{\text{true}}(t - t_{\text{last}}), \quad (4.12)$$

where t_{last} is the time of the last jump, which is typically more than one Rabi cycle before t . With this state the average purity (for the long time limit) can be estimated as

$$p = \frac{\Omega}{2\pi} \int_0^{2\pi/\Omega} \frac{1 + z(s)^2}{2} ds = \frac{3}{4}. \quad (4.13)$$

From Fig. 4, it is also observed that the simulated ensemble average variance V is approximately constant for all time. In fact, given that the no information about the sign of Ω is determinable, and that the initial distribution $P_0(\Omega)$ is symmetric, it is easy to prove that V is exactly constant.

For the third parameter ΔI , it is observed that, on average, direct detection yields information about Ω as time increases, for both initial states. It is observed that the initial slope of ΔI is zero for the ground state, while it is non-zero for the initial steady state case. The initial flatness in the first case is due to the fact that if the system starts in the ground, the rate of detections (proportional to the excited state component) scales as $(\Omega_{\text{true}}t)^2$, and with out any detections it would not be possible to gain any information. By contrast, for the steady state case there will be some excited state fraction (depending on Ω) and thus a finite detection rate even at $t = 0$. Fig. 4 also show that, after the initial flatness, the ΔI in the first case rapidly overtakes that in the second case. This

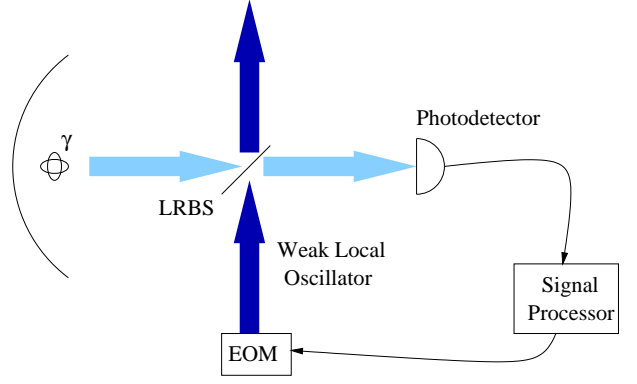


FIG. 5: A schematic for adaptive detection. The fluorescence emitted by the atom is coherently mixed with a weak local oscillator (LO) via a low reflectivity beam splitter (LRBS). The electro-optic modulator (EOM) reverses the amplitude of the LO every time the photodetector fires.

jump in ΔI occurs at roughly $t = 1/\Omega_{\text{max}}$, which is when one would expect a significant excited state fraction to have developed (Recall that $P_0(\Omega)$ is sharply peaked at $\Omega = \pm\Omega_{\text{max}}$).

B. Adaptive Detection

The second measurement scheme investigated was the adaptive scheme of Wiseman and Toombes [9]. For a known Ω , this measurement scheme is designed to keep the atom jumping between two fixed states. For Ω large, these fixed states turn out to be close to σ_x eigenstates. This two-state jumping is achieved by coherently mixing the fluorescence emitted from the atom with a weak local oscillator (LO) via a low-reflectance beam splitter (see Fig. 5). The reflected amplitude μ of the local oscillator is switched between $\pm\frac{1}{2}\sqrt{\gamma}$ each time a detection is registered by the photodetector.

For this detection scheme the measurement operators are [9]

$$M_1(dt) = \sqrt{dt\gamma}(\sigma + \mu), \quad (4.14)$$

$$M_0(dt) = 1 - (i\frac{\Omega}{2}\sigma_x + \frac{\gamma}{2}\sigma^\dagger\sigma + \mu\gamma\sigma + \frac{\gamma\mu^2}{2})dt. \quad (4.15)$$

These measurement operators result in a SME of the form

$$d\rho_{\mathbf{I},\Omega} = dN(t)\mathcal{G}[\sqrt{dt\gamma}(\sigma + \mu)]\rho_{\mathbf{I},\Omega} - dt\mathcal{H}[\zeta]\rho_{\mathbf{I},\Omega}, \quad (4.16)$$

where

$$\zeta = i\frac{\Omega}{2}\sigma_x + \frac{\gamma}{2}\sigma^\dagger\sigma + \mu\gamma\sigma + \frac{\gamma\mu^2}{2}. \quad (4.17)$$

Using the same ostensible distribution $\Lambda(r)$ as in direct detection, the LSME is

$$d\bar{\rho}_{\mathbf{I},\Omega} = dN(t)\bar{\mathcal{G}}[\sqrt{dt\gamma}(\sigma + \mu)]\bar{\rho}_{\mathbf{I},\Omega} - dt\bar{\mathcal{H}}[\bar{\zeta}]\bar{\rho}_{\mathbf{I},\Omega}, \quad (4.18)$$

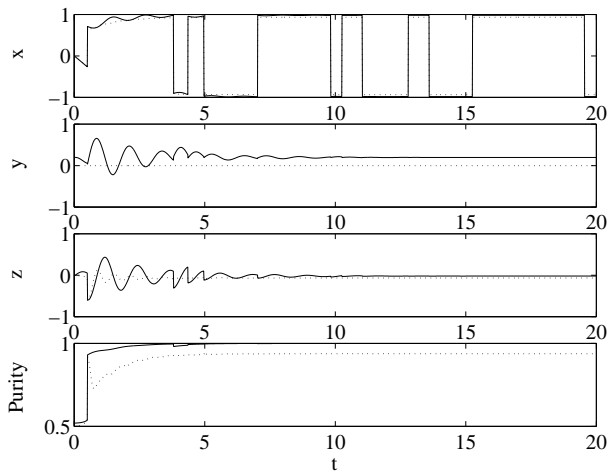


FIG. 6: The best estimate states when adaptive detection is used. Details are as in Fig. 2.

where

$$\bar{\zeta} = i\frac{\Omega}{2}\sigma_x + \frac{\gamma}{2}\sigma^\dagger\sigma + \mu\gamma\sigma + \frac{\gamma\mu^2}{2} - \frac{\epsilon}{2}. \quad (4.19)$$

Figure 6 shows the best estimate state for a known Ω (solid) and unknown Ω (dotted), with $\Omega_{\text{true}} = 5\gamma$. It is observed that with the known Ω case after the initial transients, the state jumps between the two fixed states [9]

$$x = \frac{\mp 2\Omega^2}{2\Omega^2 + \gamma^2}, \quad y = \frac{2\Omega\gamma}{2\Omega^2 + \gamma^2}, \quad z = \frac{-\gamma^2}{2\Omega^2 + \gamma^2}. \quad (4.20)$$

For the unknown Ω case the y component averages to zero, and the x and z components both appear to be slightly different to the known Ω case.

Similarly to the direct detection case, a better understanding of this state can be obtained by considering $P(\Omega|\mathbf{I}_{[0,t]})$. This is shown in Fig. 7 and it can be seen that as time increases under this adaptive measurement, the typical posterior probability distribution $P(\Omega|\mathbf{I}_{[0,t]})$ scarcely changes from $P_0(\Omega)$. This is not unexpected, as for this detection scheme it can be shown that at steady state the jumps are Poissonian, with rate $\gamma/4$. That is, the jumps are independent of Ω [9] and hence yield no information about it. Since $P(\Omega|\mathbf{I}_{[0,t]}) \approx P_0(\Omega)$, we can use this approximation to obtain analytically an indication of the best estimate state by solving Eq. (2.23). For this detection scheme this is simply the mean of Eq. (4.20) under the distribution $P_0(\Omega)$. This gives

$$x = \mp\left(1 - \frac{\gamma^2}{\sqrt{2\Omega_{\text{max}}^2 + \gamma^2}}\right), \quad y = 0, \quad z = \frac{-\gamma}{\sqrt{2\Omega_{\text{max}}^2 + \gamma^2}}. \quad (4.21)$$

Comparing this with the numerical simulation it is observed that they agree very well.

To quantify this detection scheme, the ensemble average of the variance, purity and ΔI were numerically

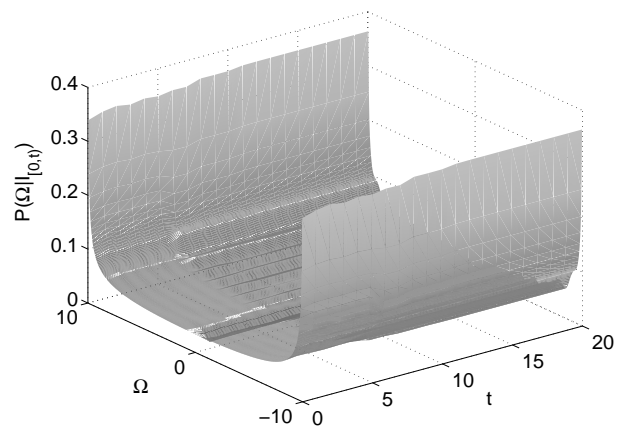


FIG. 7: A plot of $P(\Omega|\mathbf{I}_{[0,t]})$ for the adaptive scheme. Details are as in Fig. 3.

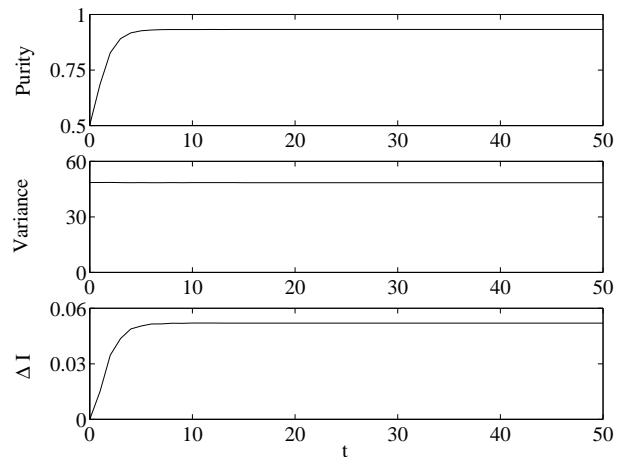


FIG. 8: The ensemble average ($n = 1000$) of the purity, variance and ΔI when the adaptive detection technique was used. Note for ΔI the scale has been change when compared to Fig. 4.

calculated and are shown in Fig. 8. The purity rapidly becomes, and remains, relatively high. This is because the best estimate state of Eq. (4.21) is the same no matter what Ω_{true} is chosen. For $\Omega_{\text{max}} = 10\gamma$ the numerical value of the stationary purity is 0.934 and by using Eq. (4.21) an analytical value of the purity can be obtained,

$$p = 1 + \frac{\gamma^2}{\gamma^2 + 2\Omega_{\text{max}}^2} - \frac{\gamma}{\sqrt{\gamma^2 + 2\Omega_{\text{max}}^2}}. \quad (4.22)$$

For $\Omega_{\text{max}} = 10\gamma$ this gives a value of 0.934, which is equal to the numerical value.

Since this state has a high purity one might expect that the unknown parameter must also be well defined. However this is not true as already discussed. This lack of knowledge about Ω is seen in Fig. 8. Like direct detection, the sign of Ω cannot be determined so the average variance remains precisely constant. However unlike di-

rect detection, the information gain is bounded, with a maximum ΔI of less than 0.06 bits.

An interesting point to note is this scheme would be well suited to estimating γ (if there were some uncertainty in that parameter) even if Ω was also uncertain. That is because the detection rate is proportional to γ , almost independent of Ω . Of course this would require the local oscillator amplitude to be adjusted from an initial guess according to the best estimate of γ .

C. Homodyne x Detection

To perform a homodyne detection experiment, a similar arrangement to the adaptive scheme is used. That is, the output flux from the atom is mixed with a resonantly tuned LO by a beam splitter (see Fig. 9). However in this scheme there is no feedback and the amplitude β of the LO is assumed to be infinite ($\beta \rightarrow \infty$). Because of this, there will be many detections in the interval dt . Each detection causes only an infinitesimal change in the system state, so the evolution of the system can be described by a diffusive SME. In each dt there will be a continuous current I registered in $\mathbf{I}_{[0,t]}$ rather than a detection or no-detection. Since I is a continuous variable we can define a measurement operator, M_I , a continuous function of I , to represent this measurement scheme,

$$M_I = \sqrt{\Upsilon_I} [1 - (i\frac{\Omega}{2}\sigma_x + \frac{\gamma}{2}\sigma^\dagger\sigma - \sqrt{\gamma}\sigma e^{-i\Phi}I)dt]. \quad (4.23)$$

Here Φ is the phase of the local oscillator and

$$\Upsilon_I dI = \frac{1}{\sqrt{2\pi/dt}} e^{-\frac{1}{2}I^2/dt} dI, \quad (4.24)$$

is a Gaussian probability measure. It is easily shown that this continuous measurement operator satisfies the completeness condition, Eq. (2.5), where the sum is replaced by an integral over I between $\pm\infty$.

With this continuous measurement operator the SME in the Itô form is [18]

$$\begin{aligned} d\rho_{\mathbf{I},\Omega} &= \mathcal{L}_\Omega \rho_{\mathbf{I},\Omega} dt + \sqrt{\gamma} \mathcal{H}[\sigma e^{-i\Phi}] \rho_{\mathbf{I}} \\ &\times (Idt - \sqrt{\gamma} \text{Tr}[\sigma e^{-i\Phi} \rho_{\mathbf{I},\Omega} + \rho_{\mathbf{I},\Omega} \sigma^\dagger e^{i\Phi}] dt), \end{aligned} \quad (4.25)$$

where I is the current element for the interval dt and is equal to the difference between the number of detections at the two photodiodes divide by the intensity of the field. By using Eq. (4.23) and Eq. (2.3) the probability of getting I for the interval dt can be calculated. This gives a Gaussian distribution with a mean equal to $\sqrt{\gamma} \langle \sigma e^{-i\Phi} + \sigma^\dagger e^{i\Phi} \rangle$ and a variance of dt^{-1} . Thus, I will be a Gaussian random variable (GRV) of the form

$$I = \sqrt{\gamma} \text{Tr}[\sigma e^{-i\Phi} \rho_{\mathbf{I}} + \rho_{\mathbf{I}} \sigma^\dagger e^{i\Phi}] + \xi(t), \quad (4.26)$$

where $\xi(t) = dW(t)/dt$ represents Gaussian white noise, and is formally defined as [21]

$$\text{E}[\xi(t)] = 0, \quad \text{E}[\xi(t)\xi(t')] = \delta(t - t'). \quad (4.27)$$

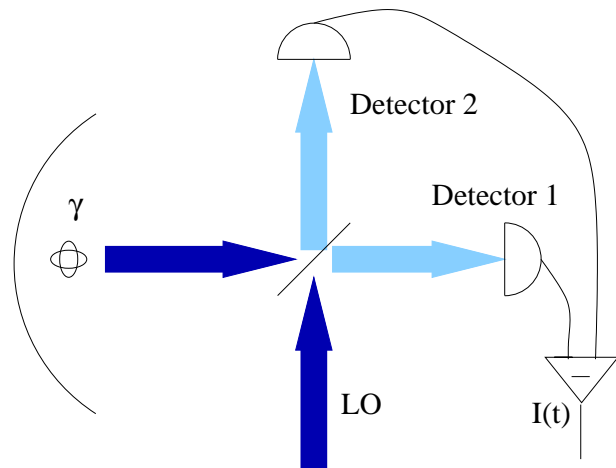


FIG. 9: A schematic for the three detection schemes, homodyne of the x quadrature, homodyne of the y quadrature and heterodyne. For the homodyne schemes the LO is resonantly tuned to the atomic frequency, with a phase of zero and $\pi/2$ for the x and y schemes respectively, whereas for the heterodyne it is detuned by an amount Δ .

For the LSME we take the ostensible probability for the current to be equal to that which would arise from the LO alone. This results in $\Lambda(I) = \Upsilon_I$ so that I is ostensibly a GRV with mean zero and variance dt^{-1} , like $\xi(t)$. The LSME in Itô form is [18]

$$d\bar{\rho}_{\mathbf{I},\Omega} = \mathcal{L}_\Omega \bar{\rho}_{\mathbf{I},\Omega} dt + \sqrt{\gamma} \bar{\mathcal{H}}[\sigma e^{-i\Phi}] \bar{\rho}_{\mathbf{I},\Omega} I dt. \quad (4.28)$$

It can be seen that both the LSME and the SME reduce to Eq. (3.1) when the ensemble average is taken. Similarly to the previous schemes, to determine an unknown Ω , $\mathbf{I}_{[0,t]}$ is generated by the SME for a preset Ω , Ω_{true} , which may then be “forgotten”. The LSME is then used to generate both $\rho_I(t)$ and $\text{P}(\Omega|\mathbf{I}_{[0,t]})$ for the predetermined record $\mathbf{I}_{[0,t]}$.

For homodyne x quadrature measurement, the Φ of the LO is set to zero (as $x = \langle \sigma + \sigma^\dagger \rangle$). With this phase and $\Omega_{\text{true}} = 5\gamma$, the best estimate state for a known and unknown Ω are shown in Fig. 10. It is observed that for the known Ω case, the state seems to localize itself relatively fast into pure states that have a large x contribution, and small oscillations in the y and z directions. By contrast, when Ω is unknown, the best estimate state still contains a large x contribution, but the y is strictly zero and the amplitude of the z oscillations is reduced. As in the previous cases, this zero y component can be understood by considering $\text{P}(\Omega|\mathbf{I}_{[0,t]})$, shown in Fig. 11. It is seen that, like direct detection, this measurement scheme has an even posterior distribution that localizes at $\pm\Omega_{\text{true}}$. This is again due to the stochastic Bloch equations being invariant under the previously considered rotational transformation. However, the rate at which this localization occurs is much slower than under direct detection.

The slower rate of information gain is confirmed with the calculation of the ensemble average of ΔI , shown in

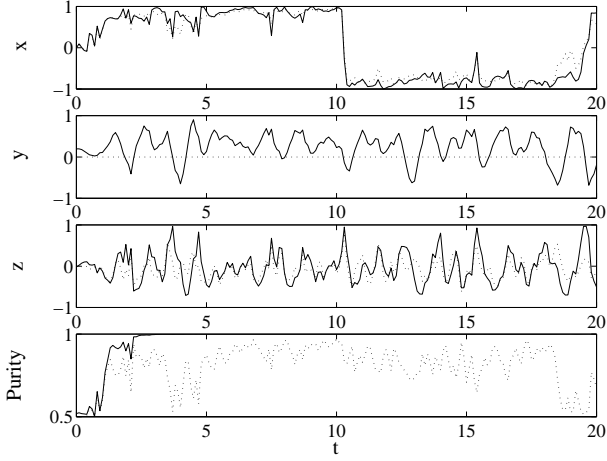


FIG. 10: The best estimate states for the homodyne x scheme. Details are as in Fig. 2.

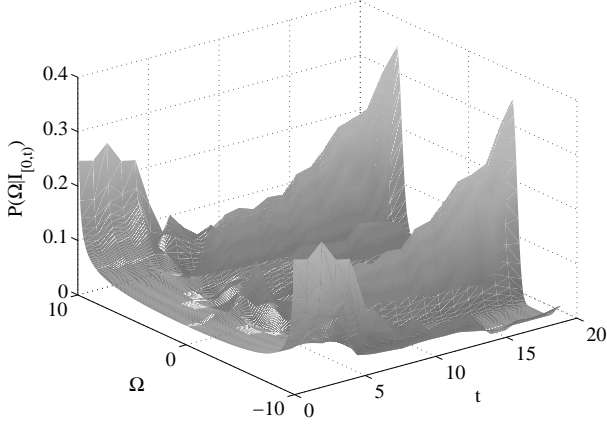


FIG. 11: A plot of $P(\Omega|\mathbf{I}_{[0,t]})$ for the homodyne x scheme. Details are as in Fig. 3.

Fig. 12. It is seen that within $50\gamma^{-1}$ units of time, ΔI for homodyne x is about half that of direct detection. Physically this comes about because, for the system we are investigating, the underlying dynamics cause the states to rotate around the x -axis with frequency Ω_{true} . The measurement scheme tends to produce states oriented mainly in the $\pm x$ directions. This can be understood from the measurement effect F_I , which, using Eq. (2.4), can be shown to be

$$F_I dI = \frac{1}{\sqrt{2\pi/dt}} e^{-\frac{1}{2}(I - \sqrt{\gamma}\sigma_x)^2 dt} dI. \quad (4.29)$$

This effect is a Gaussian with a mean equal to the σ_x quadrature operator and variance dt^{-1} . Thus, it is an unsharp measurement of σ_x . Thus, for a measurement scheme that makes the conditioned state mainly oriented in the $\pm x$ directions, one would expect that this state would be less affected by an unknown Ω than a state on the $x = 0$ plane as produced by direct detection. Thus less information about Ω comes out of the measurement

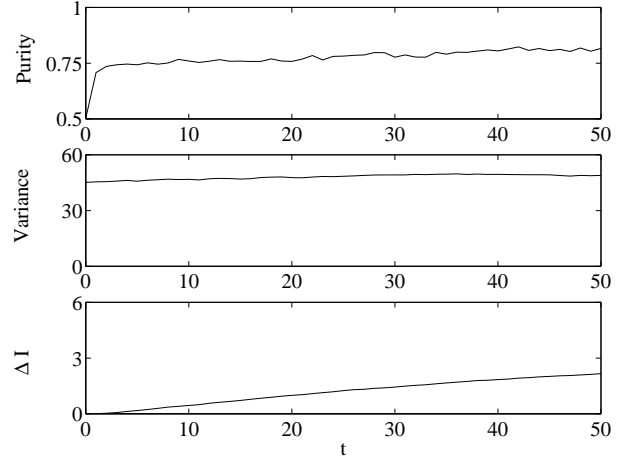


FIG. 12: The ensemble average ($n = 500$) of the purity, variance and ΔI when homodyne x was used. Time is measured in units of γ^{-1} .

record. In Fig. 11 it is observed that the ensemble average of the purity of this state increases quickly to about 0.75, then increases only slowly afterwards. This quick increase is also a result of the state becoming predominately $\pm x$ oriented. (similarly to the adaptive detection scheme) and the slow increase is due to the slow increase in the knowledge of Ω (similarly to direct detection). As with direct detection, the system state will never become fully pure. This is due to the double peaks in $P(\Omega|\mathbf{I}_{[0,t]})$, which insures the y component of the state always averages to zero.

D. Homodyne y Detection

Setting the Φ of the local oscillator to $\pi/2$ allows measurement of the y quadrature (as $y = \langle -i\sigma + i\sigma^\dagger \rangle$). The best estimate states for the known and unknown Ω are shown in Fig. 13, for $\Omega_{\text{true}} = 5\gamma$. It is seen that when Ω is known (solid) this measurement scheme makes the state coarsely rotate around the Bloch sphere with a purity of one. When Ω is unknown (dotted line), Fig. 13 shows that, unlike the previous schemes, the y component does not average to zero. As time increases the oscillations in the y and z components for the unknown Ω case gradually converge to those for the known Ω case. This suggests that this scheme can determine Ω_{true} . This is confirmed by the calculation of $P(\Omega|\mathbf{I}_{[0,t]})$ shown in Fig. 14. The ability of this scheme to distinguish the sign of Ω can be physically understood by considering the Bloch representation of Eq. (4.28). These stochastic equations are *not* invariant under the rotation transformation.

To understand how this scheme reduces the uncertainty in Ω , consider the effect for this measurement scheme

$$F_I dI = \frac{1}{\sqrt{2\pi/dt}} e^{-\frac{1}{2}(I - \sqrt{\gamma}\sigma_y)^2 dt} dI. \quad (4.30)$$

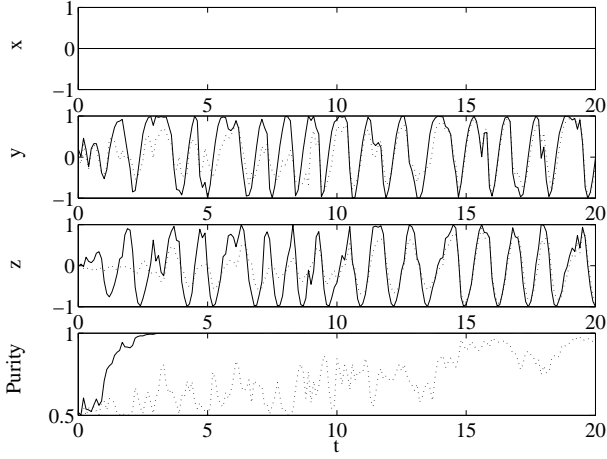


FIG. 13: The best estimate states for homodyne y measurement. Details are as in Fig. 2.

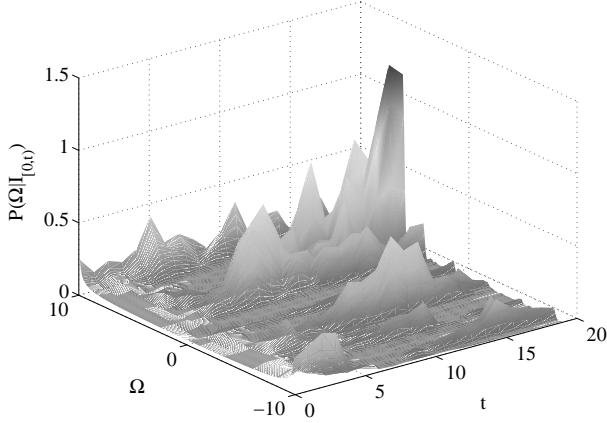


FIG. 14: A plot of $P(\Omega|\mathbf{I}_{[0,t]})$ for homodyne y measurement. Details are as in Fig. 3.

That is, F_I is an unsharp measurement of y . Now y is a variable that is directly affected by Ω_{true} , and indeed the sign of y reverses if the sign of Ω reverses. Even though in each interval dt , y is measured unsharply, over time this detection scheme will result in a narrowing of our knowledge of Ω , until infinite time where it would be fully known. This is further confirmed by the calculation of the ensemble averages of the three parameters, purity, V and ΔI (Fig. 15). It is observed that the purity of this state increases up to one, the V in Ω reduces substantially in the $50\gamma^{-1}$ units of time and ΔI increases to a value larger than that for all other schemes.

E. Heterodyne Detection

The last detection scheme considered uses the heterodyne technique. This detection scheme uses the same arrangement as the homodyne (see Fig. 9), with the only difference being that the LO is now detuned from the

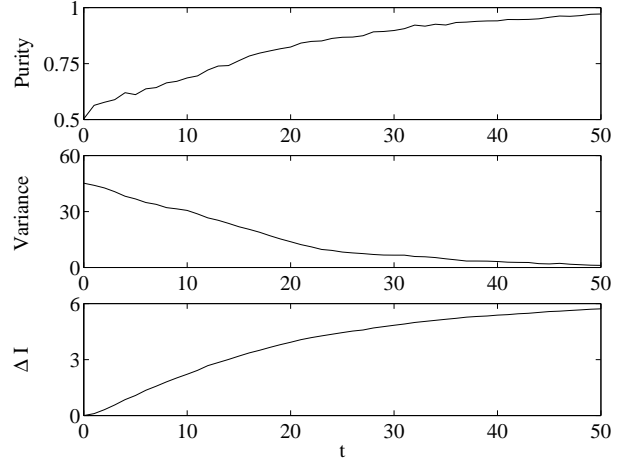


FIG. 15: The ensemble average ($n = 500$) of the purity, variance and ΔI when homodyne detection of the y quadrature was used.

atom by an amount Δ . This effectively results in the LO having a time varying phase of Δt with respect to the driving field. Since the field amplitude is still assumed to be infinite as in the homodyne case, $\mathbf{I}_{[0,t]}$ will comprise of a string of real numbers I . However, by coarse-graining to obtain the Fourier components at $\omega = \pm\Delta$, a complex photocurrent is obtained [17]. The continuous set of measurement operators after the coarse graining approximation ($\Delta dt \gg 1$ but $\gamma dt \ll 1$) are

$$M_I = \sqrt{\Upsilon_I} [1 - (i\frac{\Omega}{2}\sigma_x + \frac{\gamma}{2}\sigma^\dagger\sigma - \sqrt{\gamma}\sigma I^*)dt], \quad (4.31)$$

where

$$\Upsilon_I d^2 I = \frac{dt}{\pi} e^{-|I|^2 dt} d^2 I. \quad (4.32)$$

It is easily shown that these measurements operators satisfy the completeness condition, Eq. (2.5). To do this, one must integrate over the plane of the complex currents I .

As with homodyne, the sample path for I can be obtained from calculating the probability of getting I in the interval dt . Doing this, one obtains

$$I = [\sqrt{\gamma} \langle \sigma \rangle + \zeta(t)], \quad (4.33)$$

where $\zeta(t)$ is a complex Gaussian white noise term, which is formally defined as [21]

$$\mathbb{E}[\zeta(t)\zeta(t')] = \mathbb{E}[\zeta(t)] = 0, \quad (4.34)$$

$$\mathbb{E}[\zeta^*(t)\zeta(t')] = \delta(t-t'). \quad (4.35)$$

Using the above measurement operators and Eq. (4.33), the heterodyne SME in Itô form is [18]

$$\begin{aligned} d\rho_{\mathbf{I},\Omega} = & \sqrt{\gamma}(\sigma\rho_{\mathbf{I},\Omega} - \langle\sigma\rangle\rho_{\mathbf{I},\Omega})(I^*dt - \sqrt{\gamma}\langle\sigma^\dagger\rangle dt) \\ & + \sqrt{\gamma}(\rho_{\mathbf{I},\Omega}\sigma^\dagger - \langle\sigma^\dagger\rangle\rho_{\mathbf{I},\Omega})(Idt - \sqrt{\gamma}\langle\sigma\rangle dt) \\ & + \mathcal{L}_\Omega\rho_{\mathbf{I},\Omega}dt. \end{aligned} \quad (4.36)$$

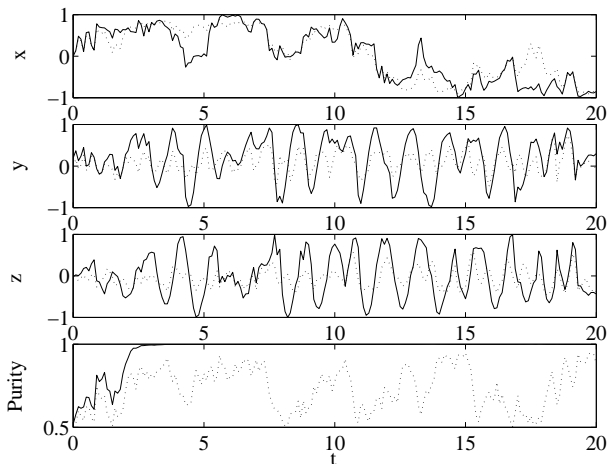


FIG. 16: The best estimate states, when heterodyne is used. Details are as in Fig. 2.

For the LSME we again assume that the ostensible probability is that due just to the LO, which results in a heterodyne current I with the same statistics as $\zeta(t)$. With this complex current the ostensible probability $\Lambda(I)$ is equal to Υ_I . This gives a LSME in Itô form of [18]

$$d\bar{\rho}_{\mathbf{I},\Omega} = \mathcal{L}_{\Omega}\bar{\rho}_{\mathbf{I},\Omega}dt + \sqrt{\gamma}\sigma\bar{\rho}_{\mathbf{I},\Omega}I^*dt + \sqrt{\gamma}\bar{\rho}_{\mathbf{I},\Omega}\sigma^\dagger Idt. \quad (4.37)$$

Using $\Omega_{\text{true}} = 5\gamma$, the best estimate state for known and unknown Ω are shown in Fig. 16. It is observed that for a known Ω , the state contains attributes of both the homodyne x and y measurement schemes. By this we mean that the state tends to have a distinct x components, whilst keeping the coarse rotations of the homodyne y scheme. This is not unexpected as heterodyne is equivalent to simultaneous homodyne x and y measurements, each of 50% efficiency [22]. In the unknown Ω case it is observed that the y component does not average to zero, suggesting that $P(\Omega|\mathbf{I}_{[0,t]})$ localizes to Ω_{true} , which is confirmed by Fig. 17. However, the rate at which $P(\Omega|\mathbf{I}_{[0,t]})$ converges to $\delta(\Omega - \Omega_{\text{true}})$ is much slower than that of the homodyne y measurement. This is also illustrated in Fig. 18 as the ensemble average ΔI is not as high. Fig. 18 also shows the ensemble average of the purity and from this figure it is seen that it contains similar properties of both the homodyne x and y schemes. In particular, it has an initial sharp increase, which is due the state obtaining a large x component (similar to the homodyne x scheme) and as time goes on the purity increases to one due to the localization of $P(\Omega|\mathbf{I}_{[0,t]})$ (similar to homodyne y).

V. DISCUSSION

The results of this paper demonstrate that quantum parameter and state estimation for a continuously monitored open system is greatly affected by the measuring scheme. It was observed that as the measurement time

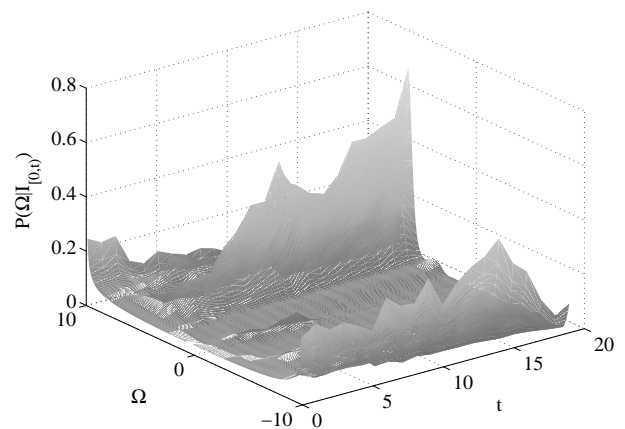


FIG. 17: A plot of $P(\Omega|\mathbf{I}_{[0,t]})$ for heterodyne detection. Details are the same as Fig. 3.

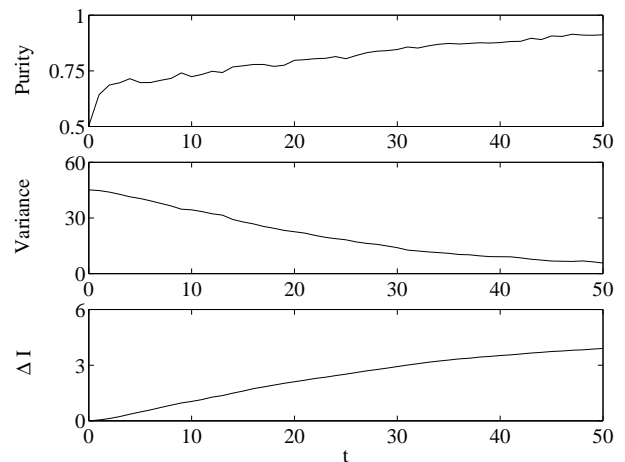


FIG. 18: The ensemble average ($n = 250$) of the purity, variance and ΔI for heterodyne detection. Time is measured in units of γ^{-1} .

increased, some detection schemes had the ability of both reducing our uncertainty in the unknown dynamical parameter, and producing a conditioned state of high purity, whereas other schemes could only do one of these, or none (depending on how the uncertainty in the unknown parameter is quantified). We re-emphasize that all of the measurement schemes arise from the same coupling of the system to the environment; all that is different is how the environment is measured.

The system we considered was a two-level atom with Hamiltonian $\Omega\sigma_x/2$, with spontaneous decay rate γ . The unknown dynamical parameter is Ω , the Rabi frequency. We began with the atom in its stationary mixed state (depending on Ω) and the prior distribution of Ω was that appropriate to an atom at a random point in a standing wave with a maximum Rabi frequency $\Omega_{\text{max}} = 10\gamma$. We analyzed five different measurement schemes, direct detection, a particular adaptive scheme [9], homodyne detection of the x quadrature, homodyne of the y , and

heterodyne. We can summarize the results of the paper using four different measures of the effectiveness of the measurement. The first two relate to the knowledge obtained about Ω . One is ΔI_l , the long-time ($t \gg \gamma^{-1}$) increase in the average information about the parameter Ω . The other is V_l , the long-time average variance in Ω . The next two relate to the knowledge obtained about the system. One is p_l , the long-time purity. This measures how much is known about the system, given the long-time knowledge about the unknown parameter Ω . The other is p_s , the short-time ($t = \text{a few } \gamma^{-1}$) purity. This time is long enough that, if Ω were known, the system would have been more-or-less completely purified, but short enough that the actual amount of information obtained about Ω is small. That is, it measures how well the measurement can purify the state despite the large initial uncertainty in the dynamics.

The results of our work is summarized in the table below, using the four measures of effectiveness for the five different detection schemes. Rather than quote figures for these four measures, we use a rating system (\star to $\star\star\star\star$), the details of which are explained in the caption. This allows the results to be taken in at a glance.

Measure	Detection Schemes				
	Direct	Adapt	Homo x	Homo y	Hetero
ΔI_l	$\star\star\star$	\star	$\star\star$	$\star\star\star\star$	$\star\star\star$
V_l	\star	\star	\star	$\star\star\star\star$	$\star\star\star$
p_l	\star	$\star\star$	\star	$\star\star\star\star$	$\star\star\star$
p_s	\star	$\star\star\star\star$	$\star\star\star$	\star	$\star\star$

TABLE I: Ratings for the five different detection schemes, for four different measures. Four \star s is the best rating and one \star the worst. For ΔI_l , any rating above \star indicates that the information about Ω continues to increase with time, with the lower cut-offs for $\star\star\star$ and $\star\star\star\star$ being $\Delta I_l = 2.5$ and 5 bits respectively at $t = 50\gamma^{-1}$. For V_l , any rating above \star indicates a variance in Ω that decreases, with the upper cut-offs for $\star\star\star$ and $\star\star\star\star$ being $V_l = \gamma^2$ and $10\gamma^2$ respectively at $t = 50\gamma^{-1}$. For p_l , a rating above $\star\star$ indicates a purity that continues to increase with time. For schemes where the purity saturates, the lower cut-off for $\star\star$ is $p_l = 0.9$. For schemes where the purity continues to increase, the lower cut-off for $\star\star\star\star$ is $p_l = 0.95$ at $t = 50\gamma^{-1}$. Finally, for p_s , the lower cut-offs for $\star\star$, $\star\star\star$, and $\star\star\star\star$ are, respectively, $p_s = 0.65, 0.75, 0.85$ at $t = 3\gamma^{-1}$. In all cases $\Omega_{\max} = 10\gamma$.

From the table it is observed that homodyne y (Sec. IV D) was the best detection scheme by all measures except for the short-time purification, for which it was the worst. Both of these aspects are explained by the fact that this scheme measures σ_y , the dynamics of which depend strongly on Ω . Hence the measurement record contains a lot of information about Ω , including its sign (because rotations over the top of the Bloch sphere are different from rotations under the bottom). This also enables the purity to approach unity as time increases. However, for short times, when little information about Ω has been obtained, a y measurement is actually very

poor for purifying the state. That is because the measurement tends to produce states with well-defined values of y , and these are states that are very sensitive to the rotation around the x -axis at rate Ω . For a poorly known Ω , this tends to make the system state more mixed, so that the purity grows only as the information about Ω increases.

After homodyne y detection, the method that provided most information about Ω was direct detection (Sec. IV A). Under direct detection, the count rate is proportional to $\sigma_z + 1$, and (like σ_y), the dynamics of σ_z depend strongly upon Ω , due to the Rabi rotations around the x -axis. However, in terms of σ_z , rotations around the $+x$ -axis from the ground state are indistinguishable from rotations around the $-x$ -axis. Hence the measurement cannot distinguish the sign of Ω and there is no change in the ensemble averaged variance as time increases. As a consequence, the purity saturates at a low value. The short time purification is poor also, for a similar reason to that for homodyne y detection.

The adaptive detection is almost complementary in its qualities to homodyne y detection. As explained in Sec. IV B, it yields almost no information about Ω , because the rate of detections in steady state is independent of Ω . In particular, it yields no information about the sign of Ω , so the variance is constant. As a consequence, the purity does not approach unity. Nevertheless, it does approach a quite high value, of over $1 - \gamma/(\sqrt{2}\Omega_{\max})$, which is 0.93 for $\Omega_{\max} = 10\gamma$. This is because the conditioned states are, for large Ω , asymptotically independent of Ω , as they approach σ_x eigenstates. This explains why the adaptive scheme gives the best results for short-time purification: the conditioned states are almost unaffected by the uncertainty in Ω .

Homodyne x detection (Sec. IV C) is in many ways similar to the adaptive scheme, and this is readily understandable since it would be expected to produce conditioned states tending towards σ_x eigenstates. Like adaptive (and direct) detection, the sign of Ω is indeterminable so the variance is constant. Hence the final purity does not approach unity. Although its asymptotic value is not as high as that for adaptive detection, it is higher than that for direct detection. This is as expected, since the conditioned states, being imperfectly localized towards the x -eigenstates, are still affected by Ω . This also explains why the initial purification is not quite as good as for adaptive detection, and why information continues to be gained (albeit slowly) as time increases.

The final scheme, heterodyne detection (Sec. IV E), is most easily understood by viewing it as an equal mixture of homodyne x and homodyne y detection, which is in fact a completely rigorous viewpoint. All of the ratings for heterodyne detection are intermediate between those for the two homodyne schemes.

In conclusion, we have shown that gaining knowledge about an unknown dynamical parameter by monitoring the system is a quite different phenomenon from gaining knowledge about the system itself. We have also dis-

tinguished different sorts of knowledge acquisition with distinct characteristics: for the unknown parameter, information gain (in bits) versus reducing the variance; and for the system, short-time purity gain versus long-time purity gain. The ability to acquire knowledge in these various ways is extremely sensitive to the choice of monitoring scheme (which does not affect the average evolution of the system). For the system we investigated, explaining the particulars of this sensitivity depends upon a detailed understanding of the conditional dynamics of the system. Our discoveries may have important implications for the suitability of different quantum feedback-

control techniques [23, 24] in experimental systems with unknown dynamical parameters. Another direction for future work could be to investigate the effect of realistic imperfections in the detection schemes on state and parameter estimation in open quantum systems.

Acknowledgments

HMW would like to acknowledge formative conversations with Andrew Doherty.

-
- [1] C.W. Helstrom, *Quantum Detection and Estimation Theory* (Academic Press, New York, 1976)
 - [2] A.S. Holevo, *Probabilistic and Statistical Aspects of Quantum Theory* (North-Holland, Amsterdam, 1982).
 - [3] J.F. Poyatos, J.I. Cirac, and P. Zoller, *Phys. Rev. Lett.* **78**, 390 (1997).
 - [4] I.L. Chuang and M.A. Nielsen, *J. Mod. Opt.* **44**, 2455 (1997).
 - [5] H. Mabuchi, *Quant. Semiclass. Opt.* **8**, 1103 (1996).
 - [6] The same idea has been considered by A. Doherty (pers. comm.).
 - [7] H.J. Carmichael, *An Open Systems Approach to Quantum Optics* (Springer-Verlag, Berlin, 1993).
 - [8] H.M. Wiseman, *Quantum Semiclass. Opt* **8**, 205 (1996).
 - [9] H.M. Wiseman and G.E. Toombes, *Phys. Rev. A* **60**, 2474 (1999).
 - [10] K. Kraus, *States, Effects, and Operations: Fundamental Notions of Quantum Theory* (Springer, Berlin, 1983).
 - [11] V.B. Braginsky and F.Y. Khalili, *Quantum Measurement* (Cambridge University Press, Cambridge, 1992).
 - [12] G.E.P. Box and G.C. Tiao, *Bayesian Interference in statistical Analysis* (Addison-Wesley, Sydney, 1973)
 - [13] P. Goetsch and R. Graham, *Phys. Rev. A* **50**, 5242 (1994).
 - [14] M.J.W. Hall, *Phys. Rev. A* **55**, 100 (1997).
 - [15] W.H. Lindblad, *Commun. Math. Phys.* **48**, 199 (1976).
 - [16] D.F. Walls and G.J. Milburn, *Quantum Optics* (Springer, Berlin, 1994).
 - [17] H.M. Wiseman and G.J. Milburn, *Phys. Rev. A* **47**, 1652 (1993).
 - [18] These equations can be derived by considering photodetection and taking the limit as the local oscillator becomes infinite [7, 19], or, more directly, by projection of the environment into eigenstates of the field quadrature [13]. Heterodyne detection can also be treated in the first way [17] or by projection onto eigenstates of the field annihilation operator [20].
 - [19] H.M. Wiseman and G.J. Milburn, *Phys. Rev. A* **47**, 642 (1993).
 - [20] H.W. Wiseman, Phd Thesis, University of Queensland (1994).
 - [21] C.W. Gardiner, *Handbook of Stochastic Methods* (Springer, Berlin, 1985).
 - [22] R. Loudon, "Quantum Noise in Homodyne Detection" in *Quantum Optics IV*, proceedings of the Fourth International Symposium, Hamilton, New Zealand, ed. J.D. Harvey and D.F. Walls (Springer, Berlin, 1986).
 - [23] H.M. Wiseman, *Modern Physics Lett. B* **9**, 629 (1995).
 - [24] A.C. Doherty, S. Habib, K. Jacobs, H. Mabuchi and S.M. Tan, *Phys. Rev. A* **62**, 012105 (2000).